PROCEEDINGS OF SCIENCE

Shock parameter dependence of electron acceleration at quasi-perpendicular collisionless shock

Fumiko Otsuka[a*], **Shuichi Matsukiyo**[a], **Mitsuo Oka**[b]

[a] *Kyushu University, 6-1 Kasuga-Koen, Kasuga, Fukuoka, Japan*

[b] *Space Sciences Laboratory, University of California, Berkeley, USA*
E-mail: otsuka@esst.kyushu-u.ac.jp

Whistler waves are important in scattering and accelerating electrons in space. In the supercritical regime where the upstream Alfvén Mach number is above the so-called whistler critical Mach number, phase standing whistler waves can be excited and confined in the foot of the quasi-perpendicular shocks. On the other hand, in the subciritical regime whistler wave trains are emitted toward the upstream of the shock. However, the electron acceleration efficiency related with the whistler critical Mach number is not understood well. Here we report new results from several 1D particle-in-cell simulations of quasi-perpendicular shocks above and below the whistler critical Mach number. In the subcritial regime, the simulation showed that high energy electrons penetrate upstream, and the density profile is similar to the standard diffusive shock acceleration. On the other hand, in the supercritical regime, the high-energy electrons are generated locally in the narrow regin of the foot or overshoot magnetic field. This is similar to electron spike events at the Earth's bow shock and interplanetary shocks. Our result will give a new insight into the understanding of electron acceleration at collisionless shocks.

38th International Cosmic Ray Conference (ICRC2023)
26 July - 3 August, 2023
Nagoya, Japan

ICRC2023
38th International Cosmic Ray Conference
The Astroparticle Physics Conference

[*] Speaker

PoS(ICRC2023)1257

1. Introduction

Acceleration of electrons at collisionless shocks is longstanding problem in the field of astrophysics and plasma physics, and there are several theoretical models and observational studies. Recently, understanding of electron acceleration at the Earth's quasi-perpendicular bow shock has progressed via Magnetospheric Multiscale (MMS) mission. Kato and Amano (2019) [1] proposed a novel theory called stochastic shock drift acceleration (SSDA) which can produce a power-law energy spectrum of electrons. This theory is a combination of the random pitch-angle scattering of electrons by plasma waves inside the shock transition region and energy gain from the motional electric field. The scattering by the plasma waves play a key role in the SSDA theory. Oka et al. (2017, 2019)[2,3] showed the observational evidences of electron scattering by high and low frequency whistler waves at the Earth's bow shock, and these observations support the SSDA theory as a promising candidate for the electron acceleration mechanism at the shock.

In fact Amano et al. (2020) [4] demonstrated, using the data detected from MMS mission, that the observed power-law energy spectrum of electrons can be explained by the SSDA theory which predict the cutoff energy of the spectrum from the observed wave amplitude. However, despite the progress, it is still unknown which mechanisms are efficient in different set of parameters for the quasi-perpendicular shocks. Oka et al.(2006) [5] conducted statistical analysis of electron acceleration efficiency at the quasi-perpendicular Earth's bow shock. The analysis revealed that the energy spectrum becomes harder for the shocks with the Alfvén Mach number above the so-called whistler critical Mach number. However, the physical reason of the observational results is not understood well.

In this paper, we discuss how the electron acceleration efficiencies are related to the whistler critical Mach number, by performing one-dimensional particle-in-cell (PIC) simulations. We found the acceleration occurs locally at the shock transition region for supercritical regime respect to the whistler critical Mach number. This is similar to the electron spike events at shocks, e.g., Tsurutani and Lin (1985) [6], Gosling et al.(1989) [7]. On the other hand, in subcritical regime, the process looks more or less the so-called diffusive shock acceleration (DSA), This numerical result is similar to the electron gradual event at the Earth's bow shock reported by Oka et al.(2009) [8] and the electron DSA event at the interplanetary shock by Shimada et al.(1999) [9].

2.Simulation setup and magnetic field overviews

To numerically produce collisionless shocks, the so-called injection method is used in one-dimensional PIC simulations. The simulation setup is the same as our paper [10]. Left of Fig. 1 shows the schematic pitcure of the method. Initially plasma consisting of electrons and ions is uniformly distributed in the one-dimensional system along the x-axis, and are drifting toward the right boundary with the drift velocity of v_{in}. Then, the reflected and incoming plasmas are mixed to produce the downstream of the shock. The shock front travels toward the left boundary with the shock velocity of $v_{sh} < 0$. Hence, the system is in the downstream rest frame, and the Alfvén Mach number is written as $M_A=(v_{in}-v_{sh})/v_A$, where v_A is the Alfvén speed. The shock speed was numerically determined by the speed of position where the magnetic field jump appeared.

Here we show three simulation runs with the parameters shown by the cross symbols in the right panel of Fig.1. For these runs, shock angle, θ_{Bn}, between shock normal x-direction and upstream magnetic field is changed, i.e. $\theta_{Bn}= 65^o$, 75^o , and 80^o. Alfvén Mach numbers are slightly different

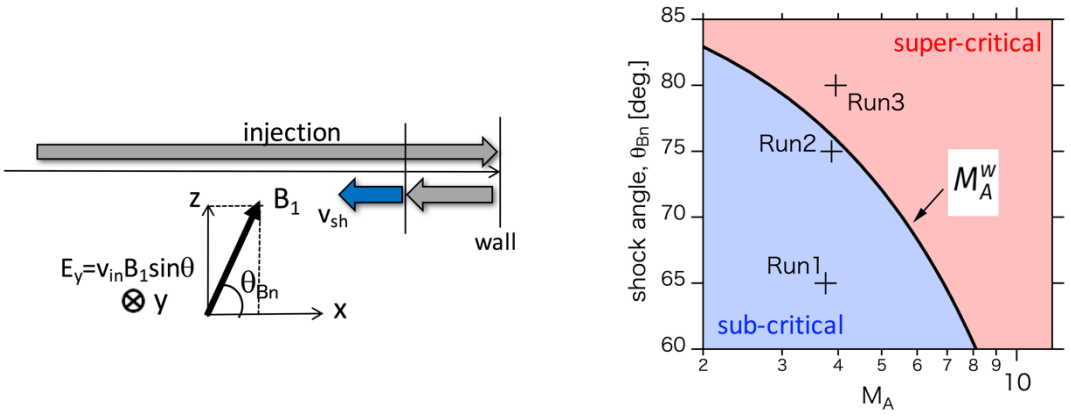

Figure 1. (left) Schematic picture of the PIC simulation setup. (right) set of parameters we performed in Alfvén Mach number and shock angle. Here the black curve indicates the whistler critical Mach number.

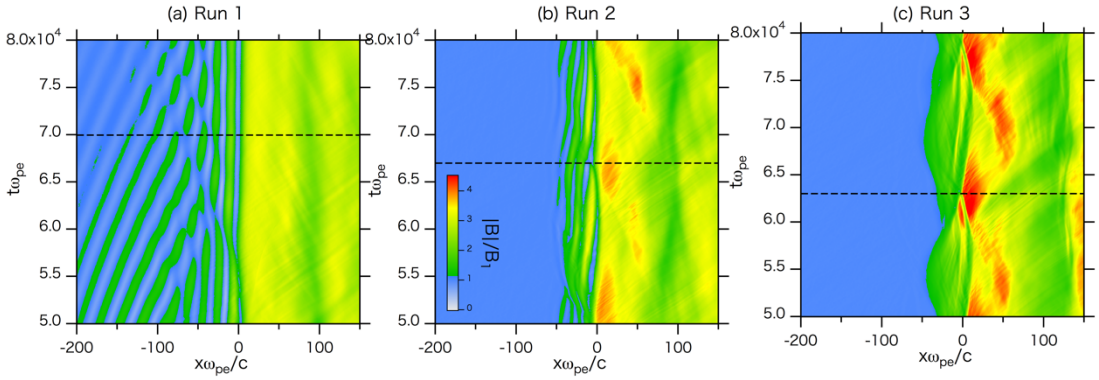

Figure 2. Spatial-temporal evolutions of the magnetic field intensity for three runs in the shock rest frame.

among three runs, because v_{sh} are slightly different values though v_{in} is the same for all runs. The parameter sets are $(\theta_{Bn}, M_A) = (65^o, 3.75)$, $(\theta_{Bn}, M_A) = (75^o, 3.86)$, and $(\theta_{Bn}, M_A) = (80^o, 3.95)$ for run 1, 2, and 3, respectively. The solid curve in the right panel of Fig.1 indicates the whistler critical Mach number defined by the maximum group velocity of the whistler wave [5].

$$M_A^w = \sqrt{\frac{27}{64}\frac{m_i}{m_e}\cos\theta_{Bn}}$$

where the superscript w stands for the whistler waves, m_i and m_e are ion mass and electron mass, respectively. Hence, run 1 is in the subcritical regime, run 2 is located around the boundary of $M_A = M_A^w$, and run 3 is in the supercritical regime.

Figure 2 shows the magnetic field intensities of three runs in space (x) and time (t) plane, where the space is defined in the shock ramp (x=0) being at rest. At subcritical regime, $M_A < M_A^w$, upstream flow speed is below the whistler group velocity, so that whistler wave trains can be emitted toward the upstream (Fig.2a). On the other hand, at supercritical regime, $M_A > M_A^w$, whistler wave cannot propagate upstream, but the phase-standing whistler wave can be excited around the foot of the shock (Fig.2b,c). This is because the flow is slow down at the foot, and its speed is locally comparable with the magnitude of the whistler group velocity, resulting in the standing wave.

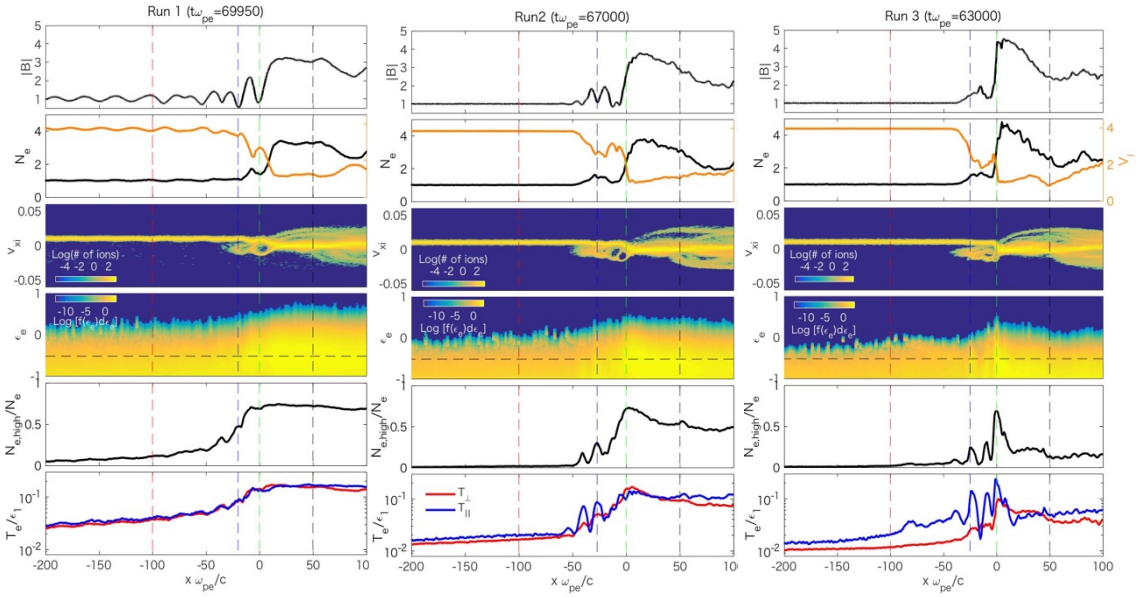

Figure 3. Snapshots of the three runs. From top to bottom, (1) magnetic field intensities, (2) electron number densities (left axis) and flow speed shown by the orange lines (right axis), (3) number of ions in the phase-space (v_x-x), (4) electron energy spectra, (5) density rate of high energy electron, (6) electron temperature perpendicular (red) or parallel (blue) to the local magnetic field.

For runs 2 and 3, overshoot magnetic field cyclically appears with the time scale of $15000/\omega_{pe}=2.4/\Omega_{i1}$, as a result of the shock reformation.

The other plasma parameters are the same for three runs as follows. The ion-to-electron mass ratio is $m_i/m_e=625$, the electron plasma frequency is $\omega_{pe}=10\ \Omega_e$, where Ω_e is electron gyrofrequency. From the parameters above, the Alfvén speed becomes $v_A=0.004\ c$, where c is the light speed. The time step and spatial grid are $\omega_{pe}\ \Delta t=0.025$, and $\Delta x=0.025\ c/\omega_{pe}$. The system length is $5000\ c/\omega_{pe}$. The upstream flow speed in the simulation frame is $v_{in}=0.01c$, so the upstream flow speed in the shock rest frame is written as $v_1=v_{in}-v_{sh}$. The plasma betas for electrons and ions are 0.15, respectively, where the beta is the ratio of the plasma pressure to the magnetic pressure. Thus, the electron beta is rewritten as $\beta_e=2T_e / m_i v_A$, where T_e is the electron temperature. In the simulation the temperature is normalized by the the upstream flow energy in the shock rest frame defined as $\varepsilon_1=m_i\ c^2(\gamma_1-1)$ where $\gamma_1=(1-\ v_1^2/c^2)^{-1/2}$. Then, the initial and injected electron temperatures normalized by ε_1 become $(v_A^2/c^2)\beta_e/2(\gamma_1-1)=0.01$.

3. Results

Figure 3 shows the snapshots of various physical values for three runs. The horizontal axis is the space in the shock rest frame as the same of Fig.2. The plotted time of these snapshots is shown by horizontal dashed lines in each run of Fig.2. From top to third panels, well-known shock structures are seen. The larger amplitude of overshoot magnetic field appears at larger θ_{Bn}. Correlated with the magnetic field profiles, the electron density and ion flow speed are discontinuously increased and decreased at shock transition region, respectively. The ion reflection at the shock produces the foot structure of the shock.

Here we focus on the electron dynamics. Forth panels of Fig.3 show the dynamic spectra of electron energy, where the electron enrgy, ε_e, is defined at the shock rest frame, and is normalized

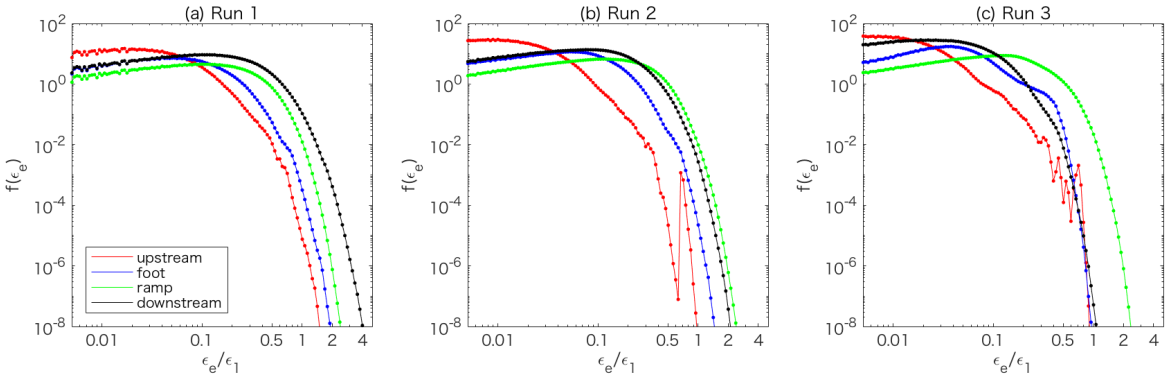

Figure 4. Electron energy spectra at the positions shown by the vertical colored lines in each run of Fig.3.

by ε_1. For the subcritical regime (run 1), the high energy electrons (light yellow) appears in a wide region downstream, while for the supercritical regime (run 3), the high energy electrons are localized around the shock transition region.

The densities for the electron with the energy higher than $\varepsilon_e=0.3\varepsilon_1$ are shown in the fifth panels. These densities are normalized by the local electron densityies shown in the second panels. The high energy density profile for run 1 looks more or less the profile predicted by the DSA. Namely, it is composed of an gradual, exponential profile upstram and constant profile downstream. The density rate of high energy electron is achived at 70% of the total electron density for the downstream of the subcritical shock. On the other hand, for the supercritical shock, the high-energy electron spikly appears only around the shock transition region.

The bottom panels show the electron temperature profiles. Here, the temperature is calculated from the variances of the electron velocities, transformed to the axes parallel and perpendicular to the local magnetic field. The perpendicular and parallel temperatures are shown by the red and blue lines, respectively. The temperature profiles are roughly correlated with the rate of high energy electron density (fifth panels). For the subcritical shock (run 1), the temperatures, $T_\perp$ and $T_\parallel$, are almost same, representing an isotropic thermalization. For the supercritical shock (run 3), $T_\parallel$ is larger than $T_\perp$ in the upstream region, representing that the shock-reflected beam electrons are thermalized well. Further, $T_\parallel$ is locally increased at foot and ramp regions. The temperature $T_\perp$ at $x=-200c/\omega_{pe}$ is around 0.01, which is the same as the initial electron temperature, representing no perpendicular thermalization upstream.

Figure 4 shows the electron energy spectra, slices of the images of forth panels of Fig.3. The sliced positions are shown by hirozontal dashed colored lines in Fig.3. The colors of the spectra in Fig.4 correspond to the positions shown in Fig.3. For run 1 (subcritical shock), the spectra look Maxwellian distriubtions with the temperature increased toward the downstream. For the foot region of run 2 and 3, there are the bumps probably corresponding to the field aligned beam electrons. Further, for run 3, the most extended energy spectrum is obtained at the shock ramp (green). This result also exhibits that the acceleration or thermalization occur locally around the shock front. The most highest energy was attained at the downstream of the subcritical shock (run 1, black). The achived highest energy is 4 times of the incoming ion enrgy, ε_1. For all three runs, we could not observe power-law energy spectra of electrons.

4.Summary

We performed three runs of one-dimensional particle-in-cell simulation of quasi-perpendicular collisionless shocks to discuss the relation between electron acceleration efficiency and the whistler critical Mach number. When the shock was in the subcritical regime respect to the whistler critical Mach number, the high energy density profile was similar to the DSA theory and the gradual event at the Earth's bow show [8]. The isotropic thermalization of electrons was also consistent with the DSA. Nevertheless, the electron energy spectra exhibit Maxwellian and do not have power-law shapes as expected from the DSA. On the other hand, when the shock was in the supercritical regime, the high energy electrons were generated locally at the narrow regions of the foot or overshoot magnetic field. This feature is consistent with the spike event of electron feature observed at the Earth's quasi-perpeneicular bow shock or interplanetary shocks (e.g.[6, 7]). We confirmed that the electrons are efficiently accelerated by the phase-standing whistler waves locally excited in the shock transition region (not discussed in this paper). The acceleration process by the whistler wave will be published soon elsewhere.

From our simulations, we found electron thermalization in the subcritical regime was larger than that in the supercritical regime, implying more efficient acceleration in the subcritical shock. This simulation result is inconsistent with the observational fact [5], if the observed harder power-law energy spectra in the supercritical regime can be considered as more efficient accelerations. We need more quantitative, statistical survey of the electron acceleration efficiencies. In the present simulations we could not reproduce the power-law energy spectrum of the electrons, in contrast to the observational fact. In quasi-perpendicular shocks electrons are tied to the magnetic field nearly perpendicular to the shock normal direction, so they are difficult to move across the shock many times in one-dimensional system. Hence, two-dimensional PIC simulation with a realistic parameter set should be one possibility to reproduce the power-law energy spectra, as observed in the Earth's bow shock. In addition, dependence of acceleration efficiency on the plasma beta should be analyzed, because the beta controls the shock self-reformation process which may influence the electron acceleration efficiency.

Acknowledgments

This research was partially supported by the JSPS KAKENHI Grant No. 22K03703, 19K03953, 22H01287.

References

[1] Katou and T. Amano, Theory of Stochastic Shock Drift acceleration for Electrons in the Shock Transition Region, The Astrophys J. Lett., 874:119 (12pp) 2019

[2] M. Oka, et al., *Electron Scattering by High-frequency Whistler Waves at Earth's Bow Shock*, The Astrophys J. Lett., 842:L11 (2017)

[3] M. Oka, et al., *Electron Scattering by Low-frequency Whistler Waves at Earth's Bow Shock*, The Astrophys J. Lett., 886:53 (11pp) 2019

[4] T. Amano et al., Observational Evidence for Stochastic Shock Drift acceleration for Electrons at the Earth's Bow Shock, Phys. Rev. Lett, 24,065101 (2020).

[5] M. Oka, et al., *Whistler critical Mach number and electron acceleration at the bow shock: Geotail observation* , Geophys. Res. Lett. 33, L24104 (2006)

[6] B.T. Tsurutani and R.P. Lin, *Acceleration of >47 keV ions and >2 keV electrons by interplanetary shocks at 1 AU, J. Geophys. Res.,* 90, A1, 1-11 (1985)

[7] J.T. Gosling, M.F. Thomsen, and S.J. Bame, *Suprathermal Electrons at Earth's Bow Shock, J. Geophys. Res.,* 94, A08, 10,011-10,025 (1989)

[8] M. Oka, et al., *Non-thermal electrons at the Earth's bow shock: A 'gradual' event*: *Geotail observation*, Geophys. Res. Lett. 33, L24104 (2009)

[9] N. Shimada, et al., *Diffusive shock acceleration of electrons at interplanetary shock observed on 21 Feb 1994*, Astrophysics and Space Science 264: 481-488 (1999)

[10] F. Otsuka et al., *Bursty betatron acceleration of electrons at nonstationary quasi-perpendicular shocks*, proceedings of 37th International Cosmic Ray Conference (2021)